

Anomalous Skew-Scattering Nonlinear Hall Effect and Chiral Photocurrents in \mathcal{PT} -Symmetric Antiferromagnets

Da Ma,^{1,*} Arpit Arora,^{1,*} Giovanni Vignale,² and Justin C. W. Song^{1,†}

¹*Division of Physics and Applied Physics, School of Physical and Mathematical Sciences, Nanyang Technological University, Singapore 637371*

²*The Institute for Functional Intelligent Materials (I-FIM), National University of Singapore, 4 Science Drive 2, Singapore 117544*

 (Received 26 January 2023; revised 31 May 2023; accepted 11 July 2023; published 17 August 2023)

Berry curvature and skew scattering play central roles in determining both the linear and nonlinear anomalous Hall effects. Yet in \mathcal{PT} -symmetric antiferromagnetic metals, Hall effects from either intrinsic Berry curvature mediated anomalous velocity or the conventional skew-scattering process individually vanish. Here we reveal an unexpected nonlinear Hall effect that relies on both Berry curvature and skew-scattering working in cooperation. This anomalous skew-scattering nonlinear Hall effect (ASN) is \mathcal{PT} even and dominates the low-frequency nonlinear Hall effect for \mathcal{PT} -symmetric antiferromagnetic metals. Surprisingly, we find that in addition to its Hall response, ASN produces helicity dependent photocurrents, in contrast to other known \mathcal{PT} -even nonlinearities in metals that are helicity blind. This characteristic enables us to isolate ASN and establishes new photocurrent tools to interrogate the antiferromagnetic order of \mathcal{PT} -symmetric metals.

DOI: 10.1103/PhysRevLett.131.076601

Nonlinear response can be a powerful diagnostic of a material's intrinsic symmetries. A prime example is the nonlinear Hall effect that manifests in time-reversal invariant but inversion broken metals [1–13]. Arising at second order in an applied electric field, the nonlinear Hall effect is often attributed to quantum geometric properties of Bloch electrons such as the Berry curvature dipole (BCD) [3,5,6] or skew-scattering processes [7,8,11,13]. Such nonlinearities can persist even in antiferromagnets (e.g., BCD nonlinear Hall effect [14]) when both inversion (\mathcal{P}) and time-reversal (\mathcal{T}) symmetries are broken. However, an unusual situation occurs in antiferromagnets that respect the combination of \mathcal{P} and \mathcal{T} symmetries, i.e., \mathcal{PT} symmetry [15–17]. Even though antiferromagnetism breaks \mathcal{P} and \mathcal{T} symmetries simultaneously, \mathcal{PT} symmetry zeroes out net Berry flux and ensures that the BCD [17] and conventional skew-scattering nonlinearities vanish [18]. Can Berry curvature or skew scattering play any role in Hall responses of \mathcal{PT} -symmetric materials?

Here we reveal a new paradigm for nonlinear transport where skew scattering (extrinsic scattering) and Berry curvature (quantum geometric) *cooperate* to produce a second-order nonlinear Hall effect that persists in \mathcal{PT} -symmetric materials. This anomalous skew-scattering nonlinear Hall effect (ASN) arises from combining a spin-dependent anomalous velocity and a skew-scattering spin-dependent distribution, Fig. 1(b). ASN is \mathcal{T} odd, vanishing in \mathcal{T} -symmetric materials; as such, it has been neglected. However, as we argue, ASN is \mathcal{PT} even, rendering \mathcal{PT} -symmetric antiferromagnets a prime venue for its realization.

Surprisingly, ASN also mediates a helicity dependent chiral photocurrent in the metallic limit peaking in the THz. This is striking since all other known intraband

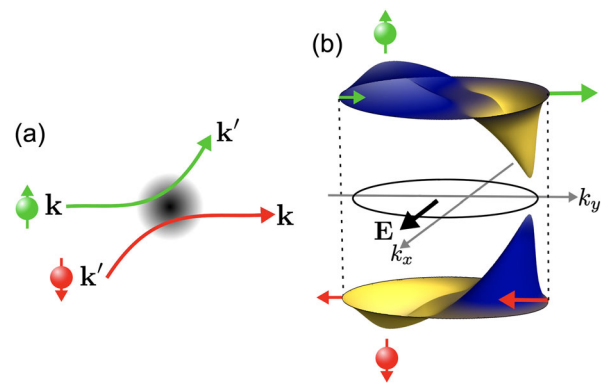


FIG. 1. Anomalous skew-scattering nonlinear Hall effect in \mathcal{PT} -symmetric materials. (a) Scattering $\mathbf{k} \rightarrow \mathbf{k}'$ for up-spin (green) shares the same rate as $\mathbf{k}' \rightarrow \mathbf{k}$ for down-spin (red) in a \mathcal{PT} -symmetric system. In particular, this \mathcal{PT} symmetry produces opposite skew-scattering contributions to the scattering rate for up- and down-spins, respectively [see Eq. (2)]. (b) Because of \mathcal{PT} symmetry, the first-order skew-scattering driven deviations of the electronic distribution (from equilibrium, solid) have opposite signs for up- and down-spins; blue and yellow indicate sign of deviation. \mathcal{PT} symmetry also enforces opposite anomalous velocity for up- (green horizontal arrows) and down- (red horizontal arrows) spins. When this spin dependent anomalous velocity is combined with skew-scattering driven deviations of the electronic distribution, a nonvanishing nonlinear Hall effect manifests even in a \mathcal{PT} -symmetric metal.

chiral photocurrents active in metals [3,19] vanish in \mathcal{PT} -symmetric materials and are insensitive to magnetic ordering [19]. ASN, as we will see below, not only survives in \mathcal{PT} -symmetric materials but is \mathcal{T} odd, making it a useful new tool for accessing helicity dependent THz chiral photocurrents locked to magnetism.

Our work lies in the context of a recent surge of interest in second-order nonlinearities [16–22] in \mathcal{PT} -symmetric antiferromagnets (e.g., CuMnAs [23,24], MnBi₂Te₄ [25,26]); such nonlinearities can be used to detect antiferromagnetic order, see, e.g., Ref. [15]. In the metallic or intraband limit, these have largely focussed on an intrinsic nonlinear Hall (INH) effect that arises from the Berry connection polarizability tensor [16,17]. INH produces nonlinear Hall currents that are independent of the scattering time, τ . In contrast, ASN is extrinsic and depends on τ at low frequencies. As a result, ASN is expected to dominate the nonlinear Hall effect in \mathcal{PT} -symmetric antiferromagnets in the clean limit providing a much needed engineering strategy for boosting nonlinear Hall signals in \mathcal{PT} antiferromagnets [15].

\mathcal{PT} partners and spin-dependent skew scattering.—We begin by examining the effect \mathcal{PT} symmetry can have on the motion of electrons. As a simple illustration, consider the minimal Bloch Hamiltonian $H^{(0)}(\mathbf{k}) = H_{\uparrow}^{(0)}(\mathbf{k}) + H_{\downarrow}^{(0)}(\mathbf{k})$, where $s = \{\uparrow, \downarrow\}$ are spins and \mathbf{k} is the electron wave vector. \mathcal{PT} symmetry enforces double degeneracy and $(\mathbf{PT})H_{\uparrow}^{(0)}(\mathbf{k})(\mathbf{PT})^{-1} = H_{\downarrow}^{(0)}(\mathbf{k})$ [23] yielding

$$\epsilon_{\uparrow}(\mathbf{k}) = \epsilon_{\downarrow}(\mathbf{k}) = \epsilon(\mathbf{k}), \quad \langle u_{\uparrow}(\mathbf{k}) | u_{\uparrow}(\mathbf{k}') \rangle = \langle u_{\downarrow}(\mathbf{k}') | u_{\downarrow}(\mathbf{k}) \rangle, \quad (1)$$

where $|u_s(\mathbf{k})\rangle$ is a Bloch state of $H^{(0)}(\mathbf{k})$ with a spin label s . For brevity of notation, we have omitted the band index. Equation (1) conveniently relates the properties of the \mathcal{PT} partners \uparrow and \downarrow . For example, \uparrow and \downarrow share the same group velocity $\mathbf{v}(\mathbf{k}) = \partial_{\mathbf{k}}\epsilon(\mathbf{k})/\hbar$, but possess opposite Berry curvature $\mathbf{\Omega}_s(\mathbf{k}) = i\langle \nabla_{\mathbf{k}} u_s(\mathbf{k}) | \times | \nabla_{\mathbf{k}} u_s(\mathbf{k}) \rangle$ signs.

Equation (1) also constrains electronic scattering. In the presence of a scalar impurity potential V , the scattering rate in a single band is given by $W_{\mathbf{k}\rightarrow\mathbf{k}'}^s = (2\pi/\hbar) |\langle u_s(\mathbf{k}') | V | \psi_s(\mathbf{k}) \rangle|^2 \delta[\epsilon_s(\mathbf{k}) - \epsilon_s(\mathbf{k}')] [27]$ that captures skew-scattering processes that occur beyond the Born approximation. Here $|\psi_s(\mathbf{k})\rangle$ is an eigenstate of the full Hamiltonian $H^{(0)}(\mathbf{k}) + V$ and can be expanded order by order using the self-consistency relation: $|\psi_s(\mathbf{k})\rangle = |u_s(\mathbf{k})\rangle + [\epsilon_s(\mathbf{k}) - H_0(\mathbf{k}) + i\eta]^{-1} V |\psi_s(\mathbf{k})\rangle [27]$. For scalar impurities and elastic scattering, we find (see Supplemental Material [28]),

$$W_{\mathbf{k}\rightarrow\mathbf{k}'}^{\uparrow} = W_{\mathbf{k}'\rightarrow\mathbf{k}}^{\downarrow}, \quad w_{\uparrow,\mathbf{k},\mathbf{k}'}^{(S,A)} = \pm w_{\downarrow,\mathbf{k},\mathbf{k}'}^{(S,A)}, \quad (2)$$

where $w_{s,\mathbf{k},\mathbf{k}'}^{(S,A)} = [W_{\mathbf{k}'\rightarrow\mathbf{k}}^s \pm W_{\mathbf{k}\rightarrow\mathbf{k}'}^s]/2$ are the symmetric and skew (antisymmetric) scattering contributions to the total

scattering rate, respectively. Crucially, the scattering process $\uparrow, \mathbf{k} \rightarrow \uparrow, \mathbf{k}'$ is the \mathcal{PT} partner of $\downarrow, \mathbf{k}' \rightarrow \downarrow, \mathbf{k}$ and have the same rate [Fig. 1(a)]. As a result, the \uparrow, \downarrow have *opposite* skew-scattering contributions. This conclusion persists for any \mathcal{PT} -symmetric scattering potential.

Equation (2) applies order by order in V , and can be obtained by applying Eq. (1) to the scattering rate. For an intuitive illustration of the origins of Eq. (2), we examine the familiar third order in V expression for the skew-scattering rate [27,33,34],

$$w_{s,\mathbf{k},\mathbf{k}'}^A = \frac{4\pi^2 n_i V_0^3}{\hbar} \sum_{\mathbf{k}''} \delta_{\mathbf{k},\mathbf{k}'}^{(\epsilon)} \delta_{\mathbf{k},\mathbf{k}''}^{(\epsilon)} \text{Im}\{L_s(\mathbf{k}, \mathbf{k}'', \mathbf{k}')\}, \quad (3)$$

where V_0 is the impurity strength, n_i the impurity density, $\delta_{\mathbf{k},\mathbf{k}'}^{(\epsilon)} = \delta[\epsilon(\mathbf{k}) - \epsilon(\mathbf{k}')]$, and $L_s(\mathbf{k}, \mathbf{k}'', \mathbf{k}') = \langle u_s(\mathbf{k}) | u_s(\mathbf{k}'') \rangle \langle u_s(\mathbf{k}'') | u_s(\mathbf{k}') \rangle \langle u_s(\mathbf{k}') | u_s(\mathbf{k}) \rangle$ is the Wilson loop associated with the Pancharatnam-Berry phase of the skew-scattering process [34]. Directly applying Eqs. (1) to (3) yields a sign changing w^A in Eq. (2). The inclusion of both \mathcal{PT} partners (in our case, spin) is essential since applying the same reasoning to a spinless system produces a vanishing w^A (e.g., Ref. [18] computed a vanishing w^A to V^4 in a spinless system).

Equations (1) and (2) have a profound impact on transport behavior of \mathcal{PT} -symmetric materials (e.g., \mathcal{PT} -symmetric antiferromagnets). Because $\mathbf{\Omega}_{\uparrow}(\mathbf{k}) = -\mathbf{\Omega}_{\downarrow}(\mathbf{k})$, the net Berry flux and the net Berry curvature dipole (BCD) vanish thereby zeroing out the intrinsic linear anomalous Hall as well as the BCD nonlinear Hall effect. Similarly, the changes to the distribution function due to skew scattering in Eq. (2) are opposite for \uparrow and \downarrow [see Fig. 1(b) and detailed discussion below]; when combined with $\mathbf{v}(\mathbf{k}) = \partial_{\mathbf{k}}\epsilon(\mathbf{k})/\hbar$, the conventional skew-scattering anomalous Hall effect at both linear and second order vanishes under \mathcal{PT} symmetry.

Anomalous skew-scattering nonlinear Hall effect.—However, when both Berry curvature mediated anomalous velocity (\mathcal{PT} odd) as well as the changes to the distribution function driven by skew scattering (\mathcal{PT} odd) combine, a nonvanishing second-order ASN Hall effect (\mathcal{PT} even) can be produced [Fig. 1(b)]. To see this in a systematic fashion, we analyze the net charge current

$$\mathbf{j}(t) = -e \sum_{\mathbf{k},s} (\mathbf{v}(\mathbf{k}) + e\mathcal{E}(t)/\hbar \times \bar{\mathbf{\Omega}}_s(\mathbf{k})) f_s(\mathbf{k}, t), \quad (4)$$

where $-e < 0$ is the carrier charge, $\mathcal{E}(t)$ is a time-varying uniform electric field, $f_s(\mathbf{k}, t)$ is the distribution function, and $\bar{\mathbf{\Omega}}_s(\mathbf{k})$ is the modified Berry curvature that includes both intrinsic Bloch band Berry curvature $[\mathbf{\Omega}_s(\mathbf{k})]$ as well as field-induced corrections [16,17,35]

$$\bar{\mathbf{\Omega}}_s(\mathbf{k}) = \mathbf{\Omega}_s(\mathbf{k}) + \nabla_{\mathbf{k}} \times \mathcal{G}(\mathbf{k})\mathcal{E}(t). \quad (5)$$

Here $\mathcal{G}(\mathbf{k})$ is the Berry-connection polarizability tensor in the metallic band of interest [16,17,35]. For band n , $[\mathcal{G}]_{ab}(\mathbf{k}) = 2e\text{Re}\{\sum_{n' \neq n} A_a^{nn'}(\mathbf{k})A_b^{n'n}(\mathbf{k})/[\epsilon_n(\mathbf{k}) - \epsilon_{n'}(\mathbf{k})]\}$, with $A_b^{nn'} = \langle u_n(\mathbf{k}) | i\partial_{k_b} | u_{n'}(\mathbf{k}) \rangle$. Here, a, b denotes Cartesian coordinates and $\mathcal{G}(\mathbf{k})$ is even under \mathcal{PT} .

For clarity, we concentrate on the intraband limit and focus on scalar impurities that preserve \mathcal{PT} symmetry and conserve spin. The distribution function in Eq. (4) can be directly computed via a spatially uniform kinetic equation, $\partial_t f_s(\mathbf{k}, t) - e\mathcal{E}(t) \cdot \partial_{\mathbf{k}} f_s(\mathbf{k}, t) / \hbar = I\{f_s(\mathbf{k}, t)\}$, where [27,36,37]

$$I\{f_s(\mathbf{k}, t)\} = \sum_{\mathbf{k}'} [W_{\mathbf{k}' \rightarrow \mathbf{k}}^s f_s(\mathbf{k}', t) - W_{\mathbf{k} \rightarrow \mathbf{k}'}^s f_s(\mathbf{k}, t)] \quad (6)$$

describes the spin-dependent collision integral.

The distribution function can be solved in the standard perturbative fashion: in powers of \mathcal{E} and for weak skew scattering by using the relaxation time approximation, see Supplemental Material for a detailed derivation [28]. As such, we expand $f_s(\mathbf{k}, t)$ as

$$f_s(\mathbf{k}, t) = f_0(\mathbf{k}) + \sum_{\ell, m} f_{\ell, s}^{(\ell, m)}(\mathbf{k}, t), \quad (7)$$

where the second term captures the deviation of the distribution function from the equilibrium distribution function, $f_0(\mathbf{k})$. Here subscript $\ell = 1, 2, \dots$ denote order in \mathcal{E} and the superscript $m = 0, 1, \dots$ denote its dependence on the skew-scattering rate; $m = 0$ captures the purely symmetric part independent of skew scattering.

Note $f_0(\mathbf{k})$ is the same for both \uparrow and \downarrow due to \mathcal{PT} symmetry. Similarly, even as $m = 0$ contributions depend on the (transport) relaxation time: $(\tau^s)^{-1} = \langle \sum_{\mathbf{k}'} w_{s, \mathbf{k}, \mathbf{k}'}^s (1 - \cos \theta_{\mathbf{v}\mathbf{v}'}) \rangle$, \mathcal{PT} symmetry in Eq. (2) ensure $f_{\ell, s}^{(0)}(\mathbf{k}, t)$ are the same for \uparrow and \downarrow since $\tau^\uparrow = \tau^\downarrow = \tau$. Here $\theta_{\mathbf{v}\mathbf{v}'}$ is the angle between $\mathbf{v}(\mathbf{k})$ and $\mathbf{v}(\mathbf{k}')$, and $\langle \dots \rangle$ indicates an average over an energy contour. In contrast, skew-scattering ($m = 1$) contributions to the distribution function $f_{\ell, s}^{(1)}(\mathbf{k}, t)$ have opposite signs for opposite spins, see Fig. 1(b): a property key to ASN.

Writing $\mathcal{E}(t) = \mathbf{E}e^{i\omega t} + c.c.$ and substituting the distribution functions into Eq. (4) enables us to directly discern the nonlinear Hall responses. Among the possible second-order nonlinear Hall responses obtained (see Table I), two are \mathcal{PT} even; the rest are odd. The first \mathcal{PT} -even response is the intrinsic nonlinear Hall (INH) effect [16,17,35] obtained by combining the second term in Eq. (5) with $f_0(\mathbf{k})$. This yields an INH current $[j^{\text{INH}}]_a(t) = \text{Re}(j_a^0 + j_a^{2\omega} e^{i2\omega t})$ with $j_a^0 = \chi_{abc}^{\text{INH}} [E_b]^* E_c$ and $j_a^{2\omega} = \chi_{abc}^{\text{INH}} E_b E_c$, where χ_{abc}^{INH} [16,17,35] depends only on band geometric quantities. χ_{abc}^{INH} is independent of τ and insensitive to ω in the semiclassical limit.

TABLE I. Symmetry of intraband nonlinear Hall responses. + indicates the response is even (i.e., allowed by symmetry), – means it is odd (i.e., forbidden by symmetry). Starred nonlinear Hall susceptibility is the new \mathcal{PT} -even response discussed in this work in Eq. (8) for the ASN, see also Supplemental Material [28].

Nonlinear Hall effects	\mathcal{T}	\mathcal{PT}	Refs.
Berry curvature dipole (BCD)	+	–	[3,5,6,14]
Intrinsic (INH)	–	+	[16,17]
Conventional skew scattering	+	–	[7,8,11]
Anomalous skew scattering (ASN)*	–	+	This Letter

The second \mathcal{PT} -even nonlinear Hall response, ASN, is the main result of our work. This nonlinear Hall effect arises from combining $\Omega_s(\mathbf{k}) \times \mathcal{E}(t)$ with the skew distribution function $f_{1, s}^{(1)}(\mathbf{k}, t)$. This produces a nonlinear Hall response: $[j^{\text{ASN}}]_a(t) = \text{Re}(j_a^0 + j_a^{2\omega} e^{i2\omega t})$ with $j_a^0 = \chi_{abc}^{\text{ASN}} [E_b]^* E_c$ and $j_a^{2\omega} = \chi_{abc}^{\text{ASN}} E_b E_c$ with

$$\chi_{abc}^{\text{ASN}} = 2 \frac{e^3 \epsilon_{adb}}{\hbar^2} \sum_{\mathbf{k}, \mathbf{k}', s} \Omega_d^s(\mathbf{k}) \tilde{\tau}_\omega^2 w_{s, \mathbf{k}, \mathbf{k}'}^A \left[\frac{\partial f_0(\mathbf{k}')}{\partial \mathbf{k}'} \right]_c, \quad (8)$$

where $\Omega_d^s(\mathbf{k})$ denotes the d component of $\Omega_s(\mathbf{k})$, $\tilde{\tau}_\omega = \tau / (1 + i\omega\tau)$ and ϵ_{adb} is the Levi-Civita symbol. Since Ω_d^s and w_s^A are both odd under \mathcal{PT} , their product is even producing a finite extrinsic nonlinear Hall effect. Importantly, χ_{abc}^{ASN} scales as $\tau^2 w^A$ for $\omega\tau \ll 1$. As a result, χ_{abc}^{ASN} is expected to dominate the nonlinear Hall response in clean systems. At finite ω , χ_{abc}^{ASN} displays a characteristic ω dependence varying rapidly on the scale $1/\tau$ (see below); this ω dependence distinguishes it from both the ω insensitive χ^{INH} as well as interband effects that have characteristic ω dependence on the scale of interband transition energy $\epsilon_n - \epsilon_m$.

Symmetry, scattering, and chiral photocurrents.—ASN has several striking attributes. Because of its Berry curvature roots, χ_{abc}^{ASN} is antisymmetric in its first two indices yielding a nonlinear Hall effect [38] always transverse to the applied electric field. This antisymmetric nature imposes additional point-group symmetry constraints as compared to conventional skew-scattering nonlinearities [7,11,13]. For example, in two dimensions, antisymmetric nonlinear χ_{abc} requires broken rotational symmetry [3,17].

ASN's antisymmetric behavior contrasts with that of another \mathcal{PT} -even nonlinear response that arises from combining $\mathbf{v}(\mathbf{k})$ with $f_{2, s}^{(0)}(\mathbf{k}, t)$ [16,18] to produce a classical nonlinearity, $\chi_{abc}^{\text{Drude}}$. Importantly, $\chi_{abc}^{\text{Drude}}$ has a susceptibility that is completely symmetric when its indices are permuted yielding a response that need not always be transverse as required of Hall type responses [38]. Experimentally, this fully symmetric nonlinear Drude response can be weeded out via interchanging the

directions of driving field and response: symmetric χ_{abc} is even under exchange, whereas nonlinear Hall responses are odd.

Perhaps most striking is how ASN produces a helicity-dependent chiral photocurrent: $[j^\zeta]_a = (i/2)\text{Im}[\chi_{abc}](E_b^*E_c - E_bE_c^*)$. ASN chiral photocurrent arises from its part quantum geometric and part skew-scattering origins. First, since ASN depends on skew scattering χ_{abc}^{ASN} possesses *both* real and imaginary components arising from the complex valued $\tilde{\tau}_\omega^2$ in Eq. (8). Second, because ASN proceeds from the anomalous velocity $\mathbf{\Omega} \times \mathbf{E}$, its susceptibility is asymmetric allowing for a nonzero \mathbf{j}^ζ after both b and c indices are summed.

Importantly, ASN's combination of geometric nature and scattering processes is essential. For instance, even as symmetric scattering alone enables a nonlinear Drude conductivity $\chi_{abc}^{\text{Drude}}$ [16,18] that has an imaginary component, it nevertheless is completely symmetric under any interchange of indices yielding a zero \mathbf{j}^ζ . Similarly, while χ_{abc}^{INH} is also asymmetric, it nevertheless is purely real, producing helicity blind photocurrents. As a result, to our knowledge, χ_{abc}^{ASN} is the only *intradband* nonlinearity that produces a helicity dependent chiral photocurrent in \mathcal{PT} -symmetric antiferromagnets; see below for a discussion of interband effects.

ASN in two-dimensional \mathcal{PT} -even antiferromagnets.—To illustrate ASN, we adopt a minimal spinful model where both \mathcal{P} and \mathcal{T} symmetries are simultaneously broken, but composite \mathcal{PT} symmetry is preserved. \mathcal{PT} enforced doubly degenerate bands can be modeled by spinful massive Dirac fermions [23]

$$H = \hbar v k_x \sigma_x + \hbar v k_y \sigma_y + \Delta \sigma_z s_z + \hbar \beta v k_y, \quad (9)$$

where the Pauli matrices σ and s describe orbital and spin degrees of freedom, respectively. Here Δ opens up a gap, v is a velocity, and β tilts the Dirac cone. The tilt term breaks rotational symmetries but preserves \mathcal{PT} . Models like Eq. (9) were recently used to successfully capture the behavior of \mathcal{PT} -symmetric antiferromagnets [17,39]. Spinful Dirac fermions can be found in a variety of materials, e.g., CuMnAs [23,24], even-layer MnBi₂Te₄ [25,26], as well as the antiferromagnet nodal line metal MnPd₂ [40]. While we concentrate on a simple model in Eq. (9) to illustrate ASN, our conclusions persist for more complex situations, e.g., an effective model of Dirac fermions in tetragonal CuMnAs [24], see Supplemental Material [28].

Broken rotational symmetry [tilt β in Eq. (9)] is essential in enabling a nonvanishing χ^{ASN} to develop in two dimensions (see discussion above); indeed, $\beta \neq 0$ means that anomalous velocities accrued at opposite ends of the Fermi surface [see Fig. 1(b)] do not cancel. Nevertheless, the \mathcal{PT} and mirror symmetries of Eq. (9) still constrain χ^{ASN} : its only nonvanishing components are $\chi_{yxx}^{\text{ASN}} = -\chi_{xyx}^{\text{ASN}}$. To demonstrate ASN, we plot the second-order nonlinear

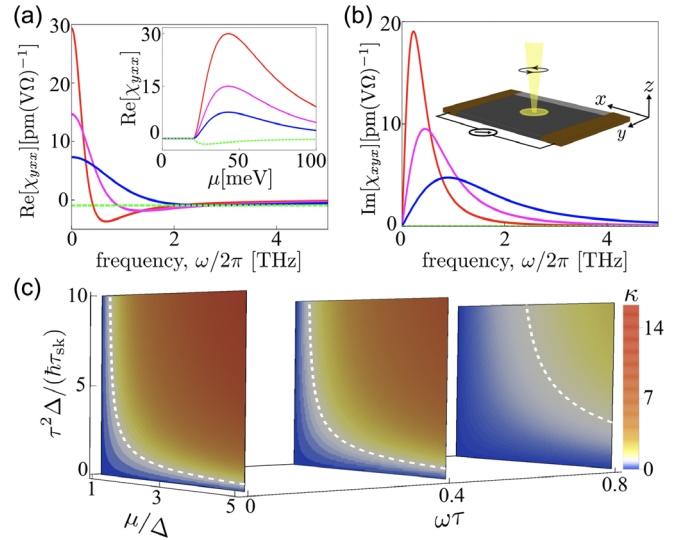


FIG. 2. ASN in a \mathcal{PT} -symmetric antiferromagnetic metal. (a) Real part of the ASN susceptibility $\chi_{yxx}^{\text{ASN}} = -\chi_{xyx}^{\text{ASN}}$ (solid lines) at different driving frequencies for Hamiltonian in Eq. (9) dominates over χ^{INH} (green dashed). (inset) $\text{Re}\chi_{yxx}^{\text{ASN}}(\omega \rightarrow 0)$ displays a peak away from the band bottom. (b) Imaginary part of ASN susceptibility can mediate a helicity dependent photocurrent (see text) and displays a maximal response at an intermediate frequency. (inset) ASN susceptibility can be isolated by probing the intraband helicity dependent photocurrent response. In both panels, red, magenta, and blue denote density of impurities set as $n_i = 1, 2, 4 (\times 10^9 \text{ cm}^{-2})$ that correspond to $\tau \approx 400, 200, 100$ fs, respectively. (c) The ratio of magnitude of ASN to INH κ , depends on dimensionless parameters see text. The dashed white curve corresponds to $\kappa = 1$. Parameters: for (a) and (b), $\Delta = 20$ meV, $\mu = 50$ meV, and $V_0 = 6.2 \times 10^{-13} \text{ cm}^2 \text{ eV}$; for all three panels, $v = 10^6$ m/s, $\beta = 0.1$.

susceptibility in Eq. (8) for chemical potential in the conduction band of Eq. (9) in Fig. 2 to leading order in β . In so doing, we have used short range impurities $V(\mathbf{r}) = V_0 \sum_j \delta(\mathbf{r} - \mathbf{r}_j)$, with strength V_0 and impurity concentration n_i , see caption for parameter values.

In the low frequency limit $\omega\tau \ll 1$, ASN scales as $\tau^2 \omega^A$ and grows with increasing τ , while INH, as an intrinsic response, is independent of τ . As a result, we find that ASN dominates the nonlinear Hall effect in clean \mathcal{PT} -symmetric materials [see Fig. 2(a)] with a peaklike structure as a function of chemical potential [Fig. 2(a)(inset)]. It displays a sensitive dependence on frequency: its real part changes sign at $\omega = 1/\tau$. This nonmonotonic dependence, as well as its τ scaling can be used as a simple diagnostic of its manifestation. In Fig. 2(c), we find that ASN dominates over wide swathes of the parameter space; the dimensionless ratio $\kappa = |\text{Re}\chi_{yxx}^{\text{ASN}}|/|\text{Re}\chi_{yxx}^{\text{INH}}|$ is controlled by three dimensionless quantities: the dimensionless Fermi level μ/Δ , dimensionless frequency $\omega\tau$, and $\tau^2\Delta/(\tau_{\text{sk}}\hbar) = \tau/\tau_{\text{sk}} \times (\tau\Delta/\hbar)$ capturing the product of the characteristic skew scattering strength and a characteristic Compton-like

scale that describes the effectiveness of the Berry curvature. We have used dimensionless quantities. Here the characteristic skew-scattering strength $\tau/\tau_{\text{sk}} = 2\pi V_0\nu(\Delta)$, where $\nu(\epsilon)$ is the density of states. The region of $\kappa > 1$ is largest at small frequencies but still covers sizable areas even for larger frequencies.

Arising from the complex valued $\tilde{\tau}_\omega^2$ in Eq. (8), $\text{Im}\chi_{abc}^{\text{ASN}}$ peaks when $\omega \sim 1/\tau$ [see Fig. 2(b)]. Strikingly, peak $\text{Im}\chi_{abc}^{\text{ASN}}$ is on par with $\text{Re}\chi_{abc}^{\text{ASN}}$ maximum. For typical τ , $\text{Im}\chi_{abc}^{\text{ASN}}$ produces a chiral photocurrent peaked in the THz regime. Interestingly, in the *interband* regime at larger frequencies, other chiral photocurrents in \mathcal{PT} antiferromagnets can also arise [19,20,41]. In particular, interband transitions can activate a circularly polarized light induced gyration current [19] that is \mathcal{PT} even but \mathcal{T} odd (also known as the circular shift photocurrent [20]); the gyration current corresponds to an imaginary nonlinear susceptibility. Importantly, gyration currents possess an ω dependence that tracks interband transitions (with characteristic scales $\omega \sim 2\Delta/\hbar$). This enables to distinguish from that of ASN chiral photocurrent that features characteristic frequency dependence in the *intradband* regime ($\omega \sim 1/\tau$), see Fig. 2(b).

ASN arises from the cooperative action of skew-scattering and Berry curvature; both are individually \mathcal{PT} odd, but when combined, produce a \mathcal{PT} -even nonlinear Hall effect that can dominate over the currently known intrinsic mechanisms [16,17] in the clean limit. This provides an engineering strategy (i.e., making the metal cleaner) for boosting the nonlinear Hall signals in \mathcal{PT} antiferromagnets for more sensitive detection. Indeed, we estimate ASN provides sizable nonlinear susceptibilities (see Fig. 2 for values) on par with those recently measured in other nonlinear materials [6]. Perhaps most striking is ASN's ability to mediate a helicity dependent photocurrent response enabling it to be directly isolated using circularly polarized drive fields. This can provide new tools for accessing a new type of quantum geometric opto-electronics [42,43] and pronounced nonlinearities in antiferromagnets.

We acknowledge useful conversations with Mark Rudner and Roberto Raimondi. This work was supported by Singapore MOE Academic Research Fund Tier 3 Grant MOE2018-T3-1-002 and a Nanyang Technological University start-up Grant (NTU- SUG).

*These authors contributed equally to this work.

†Corresponding author.

justinsong@ntu.edu.sg

- [1] J. E. Moore and J. Orenstein, *Phys. Rev. Lett.* **105**, 026805 (2010).
 [2] T. Low, Y. Jiang, and F. Guinea, *Phys. Rev. B* **92**, 235447 (2015).

- [3] I. Sodemann and L. Fu, *Phys. Rev. Lett.* **115**, 216806 (2015).
 [4] Z. Z. Du, C. M. Wang, H.-Z. Lu, and X. C. Xie, *Phys. Rev. Lett.* **121**, 266601 (2018).
 [5] Q. Ma *et al.*, *Nature (London)* **565**, 337 (2018).
 [6] K. Kang, T. Li, E. Sohn, J. Shan, and K. F. Mak, *Nat. Mater.* **18**, 324 (2019).
 [7] Z. Z. Du, C. M. Wang, S. Li, H.-Z. Lu, and X. C. Xie, *Nat. Commun.* **10**, 3047 (2019).
 [8] E. J. König, M. Dzero, A. Levchenko, and D. A. Pesin, *Phys. Rev. B* **99**, 155404 (2019).
 [9] S. Nandy and I. Sodemann, *Phys. Rev. B* **100**, 195117 (2019).
 [10] C. Xiao, Z. Z. Du, and Q. Niu, *Phys. Rev. B* **100**, 165422 (2019).
 [11] H. Isobe, S.-Y. Xu, and L. Fu, *Sci. Adv.* **6**, eaay2497 (2020).
 [12] Z. Z. Du, H.-Z. Lu, and X. C. Xie, *Nat. Rev. Phys.* **3**, 744 (2021).
 [13] P. He, G. K. W. Koon, H. Isobe, J. Y. Tan, J. Hu, A. H. C. Neto, L. Fu, and H. Yang, *Nat. Nanotechnol.* **17**, 378 (2022).
 [14] D.-F. Shao, S.-H. Zhang, G. Gurung, W. Yang, and E. Y. Tsymal, *Phys. Rev. Lett.* **124**, 067203 (2020).
 [15] J. Godinho, H. Reichlová, D. Kriegner, V. Novák, K. Olejník, Z. Kašpar, Z. Šobáň, P. Wadley, R. P. Campion, R. M. Otxoa, P. E. Roy, J. Železný, T. Jungwirth, and J. Wunderlich, *Nat. Commun.* **9**, 4686 (2018).
 [16] C. Wang, Y. Gao, and D. Xiao, *Phys. Rev. Lett.* **127**, 277201 (2021).
 [17] H. Liu, J. Zhao, Y.-X. Huang, W. Wu, X.-L. Sheng, C. Xiao, and S. A. Yang, *Phys. Rev. Lett.* **127**, 277202 (2021).
 [18] H. Watanabe and Y. Yanase, *Phys. Rev. Res.* **2**, 043081 (2020).
 [19] H. Watanabe and Y. Yanase, *Phys. Rev. X* **11**, 011001 (2021).
 [20] J. Ahn, G.-Y. Guo, and N. Nagaosa, *Phys. Rev. X* **10**, 041041 (2020).
 [21] H. Wang and X. Qian, *npj Comput. Mater.* **6**, 199 (2020).
 [22] Y. Zhang, T. Holder, H. Ishizuka, F. de Juan, N. Nagaosa, C. Felser, and B. Yan, *Nat. Commun.* **10**, 3783 (2019).
 [23] P. Tang, Q. Zhou, G. Xu, and S.-C. Zhang, *Nat. Phys.* **12**, 1100 (2016).
 [24] L. Šmejkal, J. Železný, J. Sinova, and T. Jungwirth, *Phys. Rev. Lett.* **118**, 106402 (2017).
 [25] M. M. Otrokov *et al.*, *Nature (London)* **576**, 416 (2019).
 [26] A. Gao *et al.*, *Nature (London)* **595**, 521 (2021).
 [27] N. Nagaosa, J. Sinova, S. Onoda, A. H. MacDonald, and N. P. Ong, *Rev. Mod. Phys.* **82**, 1539 (2010).
 [28] See Supplemental Material at <http://link.aps.org/supplemental/10.1103/PhysRevLett.131.076601> for additional theoretical details as well as Refs. [29–32].
 [29] N. W. Ashcroft and N. D. Mermin, *Solid State Physics* (Harcourt, Inc., New York, 1976).
 [30] P. Wadley *et al.*, *Science* **351**, 587 (2016).
 [31] P. Bhalla, K. Das, D. Culcer, and A. Agarwal, *Phys. Rev. Lett.* **129**, 227401 (2022).
 [32] P. Wadley *et al.*, *Nat. Commun.* **4**, 2322 (2013).
 [33] J. M. Luttinger, *Phys. Rev.* **112**, 739 (1958).
 [34] N. A. Sinitsyn, Q. Niu, and A. H. MacDonald, *Phys. Rev. B* **73**, 075318 (2006).

- [35] Y. Gao, S. A. Yang, and Q. Niu, *Phys. Rev. Lett.* **112**, 166601 (2014).
- [36] W. Kohn and J. M. Luttinger, *Phys. Rev.* **108**, 590 (1957).
- [37] N. A. Sinitsyn, *J. Phys. Condens. Matter* **20**, 023201 (2007).
- [38] S. S. Tsirkin and I. Souza, *SciPost Phys. Core* **5**, 039 (2022).
- [39] D. Kaplan, T. Holder, and B. Yan, *Phys. Rev. Lett.* **125**, 227401 (2020).
- [40] D.-F. Shao, G. Gurung, S.-H. Zhang, and E. Y. Tsybal, *Phys. Rev. Lett.* **122**, 077203 (2019).
- [41] P. Bhalla, K. Das, A. Agarwal, and D. Culcer, *Phys. Rev. B* **107**, 165131 (2023).
- [42] L.-k. Shi, O. Matsyshyn, J. C. W. Song, and I. S. Villadiego, *Phys. Rev. B* **107**, 125151 (2023).
- [43] Q. Ma, R. K. Kumar, S.-Y. Xu, F. H. L. Koppens, and J. C. W. Song, *Nat. Rev. Phys.* **5**, 170 (2023).